Dalton Transactions

ROYAL SOCIETY OF CHEMISTRY

PAPER

View Article Online
View Journal | View Issue



Cite this: *Dalton Trans.*, 2026, **55**, 5565

# $SnCl_2[SC(NH_2)_2]$: lone-pair and hydrogen-bonding triggered chromophore assembling for dual optical optimization

Xing-Yu Bi,†[a] Yu-Ting Gao,†[b] Chen-Yuan Ma,[a] Zhi Fang *[b] and Mei-Hong Duan *[a,c]

Received 20th January 2026,
Accepted 9th March 2026

DOI: 10.1039/d6dt00144k

rsc.li/dalton

Designing birefringent crystals with a wide bandgap presents significant challenges, especially within chalcogenide systems. Herein, motivated by the high structural anisotropy of thiourea, along with the ultraviolet compatibility and birefringence activity of halogenated tin(II)-based anionic groups, a molecular crystal-$SnCl_2[SC(NH_2)_2]$ has been screened out from crystal database. $SnCl_2[SC(NH_2)_2]$ was characterized by a bench-shaped molecular structure, which is formed by the sharing of a sulfur anion between a distorted $SnCl_2S$ trigonal pyramid and a planar π-conjugated thiourea unit. Through the synergistic interactions among multiple functional groups and the auxiliary regulation of hydrogen bonds, $SnCl_2[SC(NH_2)_2]$ succeeded in breaking the "3 eV wall" with a bandgap of 3.362 eV and achieved a large birefringence of 0.20@546 nm, demonstrating a facile design strategy for the development of chalcogenides with dual optical enhancement.



## 1. Introduction

Birefringent crystals serve as essential functional materials for manipulating the polarization state of light, demonstrating significant applications in optical isolators, optical measurements, and biomedical imaging.[1] In recent years, the rapid development of photonic technologies has intensified the demand for high-performance birefringent crystals.[2] Regrettably, commonly used birefringent crystals, including α-$BaB_2O_4$,[3] $YVO_4$[4] and $MgF_2$,[5,6] still face several limitations. For example, despite the excellent ultraviolet (UV) transmittance exhibited by $MgF_2$, practical applications of $MgF_2$ are severely restricted by its relatively small birefringence (about 0.01). Conversely, $YVO_4$ has been characterized by a giant birefringence (about 0.22), while its UV cut-off wavelength is dramatically limited to be about 400 nm. Hence, the exploration of novel birefringent crystals is still active.

Hitherto, chalcogenides have emerged as prominent candidates due to their structural diversity and excellent optical properties,[7–9] while representative crystals of $BaTeS_3$,[10] $K_2BaGeS_5$[11] and β-$Pb_3P_2S_8$[12] have been characterized by large birefringences of 0.19@550 nm, 0.19@1064 nm and 0.26@550 nm, respectively. Nevertheless, the bandgaps of chalcogenides are commonly restricted to the region below 3 eV, which poses significant challenges for their application in the UV region. To achieve transparency in the UV wavelength range, an effective approach is the introduction of strong electronegative anions ($Cl^-$, $F^-$, $O^{2-}$, $N^{3-}$, *etc.*) into chalcogenides, which has led to the development of UV-transparent chalcogenides like $La_2Zn_3(SeO_3)_6$,[13] $[Ba_4Cl_2][CdGa_4S_{10}]$,[14] $[Ba_2K][Cl][SiS_4]$,[15] $Ae_3[TO_3][SnOQ_3]$ (Ae = Sr, Ba; T = Si, Ge; Q = S, Se)[16] and $Ba_2GeF_2S_3$.[17] However, the mutual exclusivity between bandgap and birefringence leads to their birefringence being smaller than 0.1, highlighting the significance of developing chalcogenides with both large bandgaps ($E_g$ > 3 eV) and birefringences ($\Delta n$ > 0.1).

As is well known, the properties of birefringent crystals are mainly determined by the fundamental building blocks (FBBs) adopted.[18] Among various FBBs, planar π-conjugated groups have garnered much attention due to their notable structural anisotropy, potential for UV applications and tunable spatial arrangement.[19–23] Similarly, halogenated FBBs with lone pair electrons (LPE) have attracted widespread interest owing to their structural anisotropy, UV transparency and structural tunability.[24–29] Thus, we propose that the utilization of LPE-type halogenated groups to modulate planar π-conjugated sulphur-containing groups holds promise for achieving simultaneous

[a]*College of Physics and Astronomy, China West Normal University, Nanchong 637002, China. E-mail: dmh@cwnu.edu.cn*
[b]*Precise Synthesis and Function Development Key Laboratory of Sichuan Province, College of Chemistry and Chemical Engineering, China West Normal University, Nanchong 637002, Sichuan, China. E-mail: zfang@cwnu.edu.cn*
[c]*Key Laboratory of Functional Crystals and Laser Technology, TIPC, CAS, Beijing 100190, China*
† These authors contributed equally to this work.

regulation of birefringence and bandgap. Based on this hypothesis, we screened out $SnCl_2[SC(NH_2)_2]$[30] (CCDC 1120335) from the crystal database. The uniqueness of this crystal lies in the LPE-type halogenated $SnCl_2S$ triangular pyramids and planar π-conjugated sulphur-containing $SC(NH_2)_2$ molecules. Specifically, $Sn^{2+}$ is a main group cation with stereochemically active LPE, which contributes to the structural anisotropy and spatial orientation of $SnCl_2S$ groups. Meanwhile, $SC(NH_2)_2$ groups are in a quasi-coplanar alignment due to the structural modulation of $SnCl_2S$ groups, which is beneficial for optical anisotropy. Further considering the UV capability of $SnCl_2S$ groups, $SnCl_2[SC(NH_2)_2]$ is expected to achieve simultaneous regulation of birefringence and bandgap.

Herein, $SnCl_2[SC(NH_2)_2]$ crystals were synthesized using a solution volatilization method. Studies on the properties of $SnCl_2[SC(NH_2)_2]$ have indicated a large birefringence (0.2@546 nm) and a wide bandgap (3.362 eV) of $SnCl_2[SC(NH_2)_2]$, offering an effective design strategy for the development of novel UV chalcogenides with balanced bandgap and birefringence.

### 1.1. Synthesis

Analytical grade thiourea and tin(II) chloride dihydrate were procured from Shanghai Aladdin Biochemical Technology Co., Ltd and were employed without further purification. The $SnCl_2[SC(NH_2)_2]$ complex was synthesized using an aqueous solution evaporation method. Stoichiometric amounts of $SnCl_2{\cdot}2H_2O$ (0.02 mol) and $SC(NH_2)_2$ (0.013 mol) were weighed into separate beakers to afford a 2 : 1.3 molar ratio. $SnCl_2{\cdot}2H_2O$ was dissolved in 4 mL of deionized water, whereas thiourea was dissolved in the minimum volume of deionized water required for complete solvation. The two solutions were merged and subjected to magnetic stirring for 50 minutes. Subsequently, the mixture was left undisturbed in the dark at ambient temperature for a period of one week. Following this, colorless block $SnCl_2[SC(NH_2)_2]$ crystals were isolated.

### 1.2. Powder X-ray diffraction

The powder X-ray diffraction datas for $SnCl_2[SC(NH_2)_2]$ crystals were acquired under ambient conditions using a TongDa TD-3500 X-ray diffractometer, employing CuKα radiation ($\lambda$ = 1.54056 Å). The $2\theta$ angle was scanned from 10° to 70°, with a step size of 0.02° and a fixed counting time of 0.1 s per step. The $SnCl_2[SC(NH_2)_2]$ crystal powder was analyzed, and its experimental XRD pattern was compared against standard data to confirm the product's purity (Fig. 1).

### 1.3. Infrared absorption spectrum

The infrared (IR) absorption spectrum of the powder sample in the wavenumber range of 400–4000 $cm^{-1}$ was acquired using a PerkinElmer Spectrum Two Fourier Transform Infrared spectrometer.

### 1.4. UV-Vis diffuse reflectance spectroscopy

The UV-Vis reflectance spectra of the powder sample were collected in the wavelength range from 200 nm to 800 nm using a UV-2600 UV-Vis-NIR spectrophotometer, while $BaSO_4$ was selected as the reference standard.

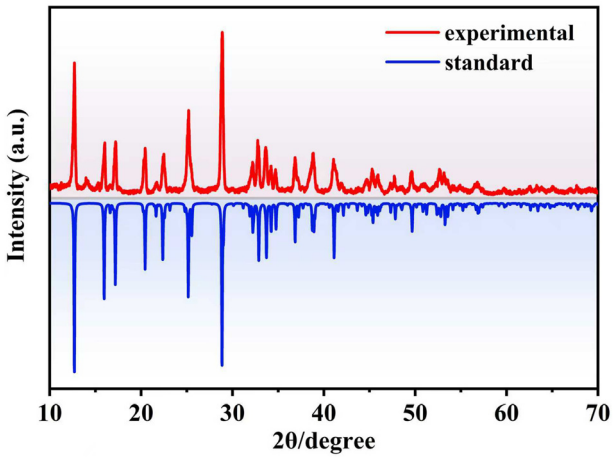


Fig. 1 PXRD patterns of $SnCl_2[SC(NH_2)_2]$.

### 1.5. Birefringence measurement

The birefringence of $SnCl_2[SC(NH_2)_2]$ crystals was determined using a polarizing microscope equipped with a Berek U-CTB compensator and a 546 nm filter, while the following equation was adopted for the assessment of the birefringence:

$$\Delta L = \Delta n \cdot d,$$

$\Delta L$ represents the optical path difference, $\Delta n$ denotes the birefringence, and $d$ indicates the crystal thickness.

### 1.6. Theoretical calculation

Theoretical predictions were conducted using plane-wave pseudopotential density functional theory (DFT).[31] The generalized gradient approximation (GGA) delineated by Perdew–Burke–Ernzerhof (PBE) was selected as the exchange–correlation functional.[32] A cutoff energy of 750 eV was applied to ascertain the number of plane-wave basis sets, while the Monkhorst–Pack $k$-point sampling for numerical integration in the Brillouin zone was established at 5 × 2 × 3. In the band structure calculations, 56 empty bands were factored in, whereas 168 empty bands were harnessed for the density of states (DOS) calculation.

## 2. Results and discussion

### 2.1. Crystal structure

$SnCl_2[SC(NH_2)_2]$ crystallized in the monoclinic space group $P2_1/c$ with cell parameters $a$ = 5.951 Å, $b$ = 13.937 Å, $c$ = 8.883 Å, $\beta$ = 111.13°, and $V$ = 687.212 $Å^3$. As illustrated in Fig. 2, $SnCl_2[SC(NH_2)_2]$ is a molecular crystal with the asymmetric unit constituted by one Sn atom, one S atom, one C atom, two Cl atoms, and two N atoms (hydrogen atoms were omitted). As illustrated in Fig. 2, all S atoms are bonded to C atoms by double bonds, and each C atom is bonded to two

 

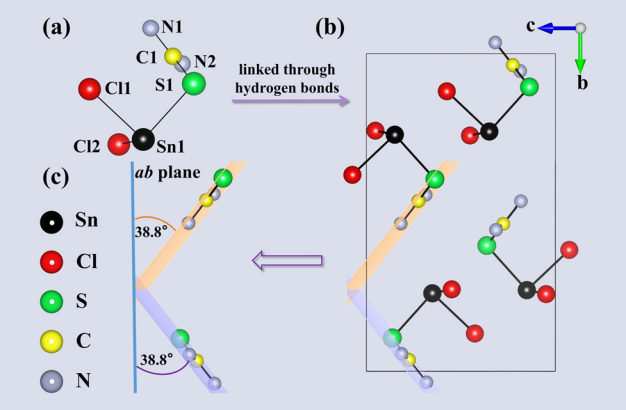


**Fig. 2** Structures of $SnCl_2[SC(NH_2)_2]$: (a) the asymmetric unit of $SnCl_2[SC(NH_2)_2]$, (b) the overall structure of $SnCl_2[SC(NH_2)_2]$, and (c) illustration of the structural configuration of thiourea groups.

$-NH_2$ groups by single bonds, ultimately forming a nearly planar $SC(NH_2)_2$ group. All $Sn^{2+}$ ions are connected to two $Cl^-$ ions and one $SC(NH_2)_2$ group to form $SnCl_2[SC(NH_2)_2]$ groups with the Sn–Cl bond lengths of 2.492(2)–2.608(3) Å and the elongated Sn–S bond length of 2.703 Å. The $SnCl_2[SC(NH_2)_2]$ group is the basic repeating unit of the $SnCl_2[SC(NH_2)_2]$ crystal. Within the $SnCl_2[SC(NH_2)_2]$ group, benefiting from the strong repulsion of the lone pair electrons from $Sn^{2+}$ and the significant bond length difference between Sn–Cl and Sn–S bonds, the $Sn^{2+}$ ion, two bonded $Cl^-$ ions, and one S atom form a markedly distorted $SnCl_2S$ trigonal pyramidal group, which is likely to make a substantial contribution to the birefringence of $SnCl_2[SC(NH_2)_2]$. On the other hand, featuring a planar π-conjugated structure, the thiourea group always acts as a birefringent active moiety. Within the crystal lattice of $SnCl_2[SC(NH_2)_2]$, all thiourea groups were linked through directional N–H···Cl hydrogen-bonding interactions with the $SnCl_2S$ trigonal pyramidal units, resulting in an ordered arrangement relative to the *ab* plane, and the bond lengths of these hydrogen bonds span 3.318(22)–3.428(4) Å, while the corresponding bond angles range from 97.0(8)° to 120.9(8)°. Besides, the dihedral angle between the thiourea molecular plane and the *ab* plane is 38.8°. This spatial packing dominated by the hydrogen bond parameters effectively amplifies the intrinsic optical anisotropy of the thiourea groups. In addition, the interconnections between groups within the $SnCl_2[SC(NH_2)_2]$ crystal endow it with a certain degree of thermal stability, and the thermal stability temperature of the $SnCl_2[SC(NH_2)_2]$ crystal can reach 160 °C (Fig. S1). Furthermore, within each $SnCl_2[SC(NH_2)_2]$ molecule, the molecular plane of the $SnCl_2$ moiety lies nearly parallel to that of the coordinated thiourea group, which is supposed to further enhance the overall birefringence of $SnCl_2[SC(NH_2)_2]$.

### 2.2. IR spectra analysis

The Fourier transform infrared (FT-IR) spectrum of the as-synthesized crystal exhibits characteristic vibrational modes corresponding to the coordination environments of Sn, S and Cl. Comparison with the IR spectrum of pure thiourea (Fig. 3) confirms the presence of thiourea groups in the structure of the $SnCl_2[SC(NH_2)_2]$ crystal. The assignments of the characteristic absorption peaks are as follows: in the high-frequency region, the absorption bands at 3382 $cm^{-1}$, 3290 $cm^{-1}$, and 3192 $cm^{-1}$ are assigned to the asymmetric and symmetric N–H stretching vibrations of the $NH_2$ group in the thiourea moiety. Upon complexation, these vibrational bands all shift to higher wavenumbers relative to free thiourea, which is attributed to the formation of the Sn–S coordination bond that enhances the contribution of highly polar resonance structures within the thiourea molecule, thereby increasing the double-bond character of the C–N bond and rendering the C=S bond more single-bond-like.[33] The strong absorption band at 1612 $cm^{-1}$ is assigned to the $NH_2$ bending vibration,[33] while the band in the 1500–1550 $cm^{-1}$ region corresponds to the N–C–N skeletal stretching vibration of the thiourea group. This band shifts from 1465 $cm^{-1}$ in free thiourea to a higher wavenumber upon coordination, also due to the enhanced double-bond character of the C–N bond.[33] The band at 1392 $cm^{-1}$ arises from the coupling of $NH_2$ wagging, N–C–N stretching, and C=S stretching vibrations. The band at 1101 $cm^{-1}$ represents a composite mode involving symmetric C–N stretching, $NH_2$ wagging, and C=S stretching vibrations; it shifts from 1093 $cm^{-1}$ in free thiourea to 1101 $cm^{-1}$ upon coordination. This blue shift can be explained by the significant reduction in the contribution of C=S stretching upon sulfur coordination, causing symmetric C–N stretching to dominate this vibrational mode. Furthermore, the absorption band at 700 $cm^{-1}$ is assigned to a coupled mode of C=S stretching and symmetric C=N stretching vibrations; its notable downshift from 730 $cm^{-1}$ in free thiourea indicates that coordination weakens the double-bond character of the C=S bond. In addition, the two weak absorption peaks of 1766 $cm^{-1}$ and 1726 $cm^{-1}$ mainly originate from the C=O stretching vibration of a small amount of urea, which is a minor hydrolysis product of thiourea.

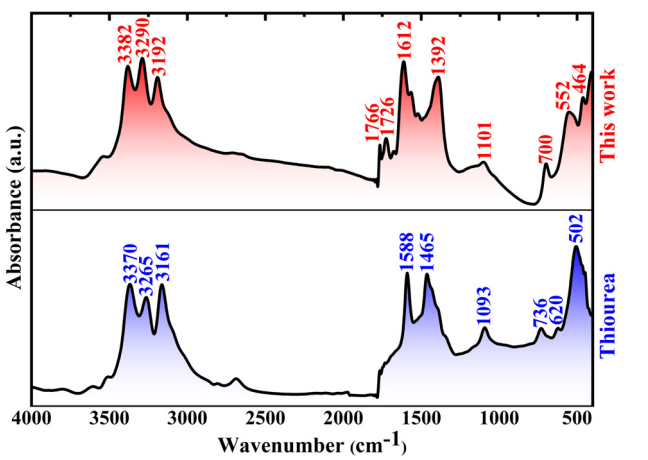


**Fig. 3** IR spectra of $SnCl_2[SC(NH_2)_2]$ and pure thiourea.

### 2.3. Optical properties

With the presence of the UV-applicable FBB of $SnCl_2$ and the UV-detrimental unit of $SC(NH_2)_2$, the optical transparency of $SnCl_2[SC(NH_2)_2]$ is of extreme significance for its practical applications. As shown in Fig. 4, the optical reflectance rate of $SnCl_2[SC(NH_2)_2]$ remains above 80% that of benchmark $BaSO_4$ in the wavelength region from 400 nm to 800 nm, indicating good transparency of $SnCl_2[SC(NH_2)_2]$ in the visible region. In contrast, the reflectance rate dropped sharply in the UV region, while the cut-off wavelength was about 320 nm. Also, with the utilization of KM fitting as shown in the inset of Fig. 4, the actual bandgap of $SnCl_2[SC(NH_2)_2]$ was determined to be 3.362 eV, a value that is larger than those of typical chalcogenides like CdS,[34] α-HgS,[35] and ZnTe[36] and rivals those of oxides like $SrTiO_3$,[37] $Nb_2O_5$,[38] and $SrSnO_3$.[39] In particular, despite the molecular crystal nature of $SnCl_2[SC(NH_2)_2]$, the bandgap of $SnCl_2[SC(NH_2)_2]$ is larger than that of pure thiourea crystals,[40] suggesting the importance of $SnCl_2$ in contributing to the wide bandgap of $SnCl_2[SC(NH_2)_2]$.

To get an idea of the optical dispersion ability of $SnCl_2[SC(NH_2)_2]$, a piece of the $SnCl_2[SC(NH_2)_2]$ crystal was selected for the measurement of the optical path difference and the corresponding crystal thickness using a polarization microscope equipped with a Bereck compensator and a 546 nm light filter. As shown in Fig. 5(a), the OPD was recorded to be 1.139 μm using the Bereck compensator when the top surface of the crystal was subjected to be in the state of total light extinction, while the crystal thickness was found to be 5.69 μm as depicted in Fig. 5(b). Hence, the birefringence ($\Delta n$) of $SnCl_2[SC(NH_2)_2]$ was calculated to be 0.20 which is much larger than those of common UV birefringent crystals like α-BBO and $MgF_2$. Also, compared with tin-based UV crystals like $Sn_2B_5O_9Cl$ (0.168@546 nm),[41] $Sn_2OSO_4$ (0.004@546 nm)[42] and $Sn_3O_2(OH)(HSO_4)$ (0.169@546 nm)[42] as well as thiourea-containing crystals like $Hg[CS(NH_2)_2]_4(SiF_6)$ (0.145@546 nm),[43] $[C(NH_2)_3]_2SiF_6$ (0.16@546 nm)[44] and $Zn[CS(NH_2)_2]_3SO_4$ (0.09@546 nm),[45] the birefringence of $SnCl_2[SC(NH_2)_2]$ has much advantage. This finding demonstrates the effectiveness of combining thiourea and LPE-type $Sn^{2+}$ in the construction of birefringent crystals for better performance.

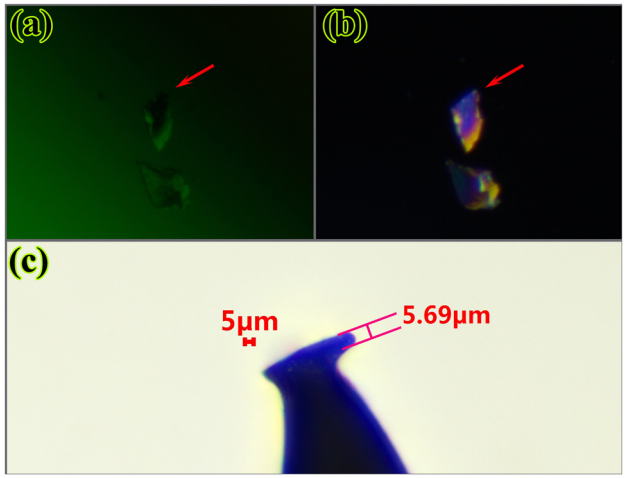


Fig. 5 Assessment of the birefringence of $SnCl_2[SC(NH_2)_2]$: (a) complete light extinction of the crystal with a 546 nm light filter, (b) the crystal under polarized illumination without a light filter, and (c) the thickness of the crystal.

### 2.4. Theoretical calculation

To elucidate the origin of the bandgap and birefringence of $SnCl_2[SC(NH_2)_2]$, first-principles calculations of the band structure, total and projected DOS, and electron-localization function (ELF) were conducted. An indirect bandgap of 2.722 eV is predicted for $SnCl_2[SC(NH_2)_2]$ (Fig. 6a), which slightly underestimates the experimental value of 3.362 eV. This underestimation of bandgap should be attributed to the discontinuity of GGA–PBE exchange–correlation potentials.[46] According to the total and projected DOS maps presented in Fig. 6b, the upper region of the valence band of $SnCl_2[SC(NH_2)_2]$ is dominated by hybridized Sn 5s–5p, S 3p and Cl 3p states, whereas the valence band maximum (VBM) is localized almost exclusively

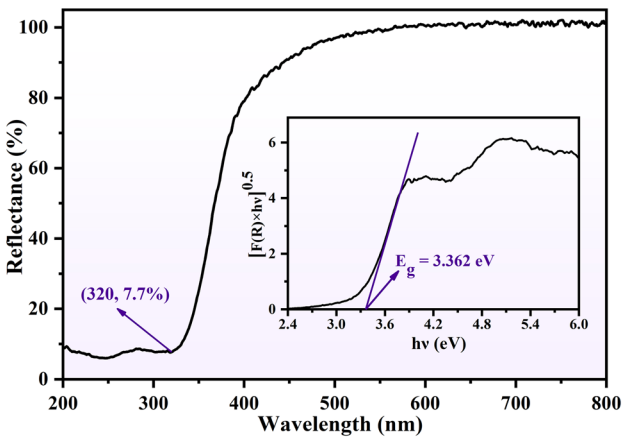


Fig. 4 UV-Vis diffuse reflectance spectrum of $SnCl_2[SC(NH_2)_2]$.

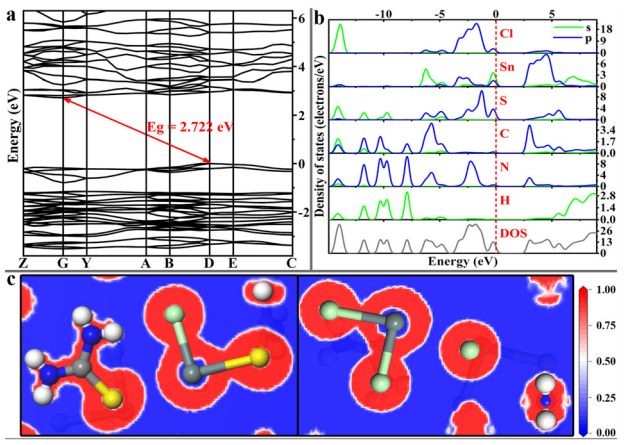


Fig. 6 Calculated band structure (a), total and projected DOS maps (b), and ELF (c) for $SnCl_2[SC(NH_2)_2]$.

on the S 3p orbitals. The bottom of the conduction band of $SnCl_2[SC(NH_2)_2]$ is constructed primarily from Sn 5p and C 2p contributions, with the conduction band minimum (CBM) occupied by Sn 5p states. Hence, the pronounced separation between the VBM and CBM is primarily attributed to the ionic bonds between Sn and S atoms, which effectively lowers the VBM, while the high-energy nature of the Sn 5p states also dictates the position of the CBM. Although $Cl^-$ anions do not directly contribute to bandgap formation, the robust Sn–Cl bonding interactions are distinctly revealed by the significant overlap of the Sn 5s–5p and Cl 3p states within the upper region of the valence band, which collaboratively facilitates the downward shift of the VBM.

As illustrated in Fig. 6c, the electron localization function (ELF) reveals pronounced anisotropy in the electron density distribution surrounding the thiourea molecular plane. This anisotropic feature highlights the critical role of thiourea in dictating the optical anisotropy of $SnCl_2[SC(NH_2)_2]$. The electron cloud behavior around the $S^{2+}$ cations shows significant anisotropy, which further substantiates thiourea's substantial contribution to the material's birefringence properties. Turning to the $SnCl_2$ moiety, no notable anisotropy is observed in the electron density surrounding the $Cl^-$ anions; however, the region adjacent to the $Sn^{2+}$ cations exhibits distinct anisotropic electron localization. This finding identifies $Sn^{2+}$ as the other key contributor to the optical dispersion capabilities of $SnCl_2[SC(NH_2)_2]$, a phenomenon attributed to the stereochemical activity of its lone pair electrons. While $Cl^-$ anions do not exert a significant influence on birefringence, strong electron localization is evident in their vicinity. This characteristic confirms that $Cl^-$ anions act as electron acceptors from Sn atoms, which facilitates the expansion of the material's bandgap. Clearly, this electron acceptance phenomenon aligns well with the DOS maps discussed earlier. Subsequently, $SnCl_2$ emerges as the critical factor in overcoming the "3 eV wall" barrier while simultaneously maintaining a well-balanced birefringence. Additionally, the calculated refractive index (Fig. S2) revealed that the birefringence of $SnCl_2[SC(NH_2)_2]$ is primarily dominated by the disparity between the refractive indices $n_y$ and $n_x$, which is consistent with the arrangement of thiourea groups within the $SnCl_2[SC(NH_2)_2]$ structure, further underscoring the pivotal role of thiourea in generating substantial birefringence.

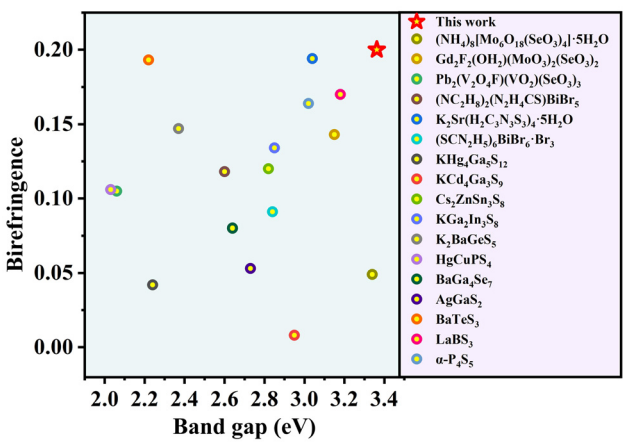


**Fig. 7** Illustration of the birefringence and bandgap of some chalcogenide crystals.

## 3. Conclusion

In summary, the molecular crystal —$SnCl_2[SC(NH_2)_2]$ has been investigated as a promising candidate for birefringent applications. This compound successfully overcomes the "3 eV wall" barrier through the unique bonding interactions and electron transfer processes between $Sn^{2+}$ cations and $S^{2-}/Cl^-$ anions. Additionally, the cooperative structural arrangement of π-conjugated thiourea planes and LPE-type $SnCl_2S$ trigonal pyramidal units played a critical role in contributing to a large birefringence of $\Delta n$ = 0.20@546 nm. When compared to typical chalcogenide birefringent crystals (as shown in Fig. 7), $SnCl_2[SC(NH_2)_2]$ exhibits a well-balanced performance between bandgap and birefringence. Consequently, the discovery of $SnCl_2[SC(NH_2)_2]$ offers an effective design strategy for developing high-performance chalcogenide birefringent crystals. Further related research efforts are currently underway.

## Conflicts of interest

There are no conflicts to declare.

## Data availability

Data supporting this article have been included as part of the supplementary information (SI). Supplementary information (SI) is available. See DOI: https://doi.org/10.1039/d6dt00144k.

## Acknowledgements

We gratefully acknowledge the support from the Sichuan Science and Technology Program (No. 2023NSFSC0957), the Natural Science Foundation of Sichuan Province (No. 2022NSFSC1854), the PhD Research Startup Foundation of China West Normal University (No. 20E070 and 22kE011) and the Key Laboratory of Functional Crystals and Laser Technology, TIPC, CAS (No. FCLT202204).

## References

1 B. Liang, J. Ji, D. Tang, Y. Huang and X. Huang, *Mater. Res. Express*, 2021, **8**, 015902.
2 A. L. Xu, M.-Y. Ran, X.-T. Wu, H. Lin and Q.-L. Zhu, *Coord. Chem. Rev.*, 2025, **540**, 216775.

3 G. Zhou, J. Xu, X. Chen, H. Zhon, S. Wang, K. Xu, P. Deng and F. Gan, *J. Cryst. Growth*, 1998, **191**, 517–519.
4 S. Wu, G. Wang, J. Xie, X. Wu and G. Li, *J. Cryst. Growth*, 2003, **249**, 176–178.
5 M. J. Bloemer and M. Scalora, *Appl. Phys. Lett.*, 1998, **72**, 1676–1678.
6 T. C. Wen and D. K. Shetty, *J. Am. Ceram. Soc.*, 2015, **98**, 829–837.
7 M. B. P. Querne, J. M. Bracht, J. L. F. Da Silva, A. Janotti and M. P. Lima, *Phys. Rev. B*, 2023, **108**, 085409.
8 P.-F. Li, C.-L. Hu, B. Zhang, J.-G. Mao and F. Kong, *Chin. Chem. Lett.*, 2026, **37**, 110588.
9 B. Zhang, W. Q. Huang, J. X. Zhang, X. T. Wu, H. Lin and Q. L. Zhu, *Angew. Chem.*, 2025, **137**, e202508555.
10 A. M. Aparna, A. Anand, S. A. Rajput and A. K. Chandiran, *ChemPlusChem*, 2025, **90**, e202500293.
11 W. Xie, F. Li, J. Chen, Z. Yang, G. Li and S. Pan, *Angew. Chem.*, 2023, **135**, e202307895.
12 W. Guo, Y. Zhu, H.-H. Cui, L. Li, Y. Yu, Z.-Z. Luo and Z. Zou, *Chin. Chem. Lett.*, 2025, **36**, 110256.
13 P.-F. Li, X.-X. Wang, C.-L. Hu, J.-G. Mao and F. Kong, *Inorg. Chem.*, 2025, **64**, 8856–8862.
14 J. X. Zhang, S. H. Zhou, X. T. Wu, H. Lin and Q. L. Zhu, *Angew. Chem., Int. Ed.*, 2025, **64**, e202506658.
15 Y.-F. Shi, S.-H. Zhou, X.-T. Wu, H. Lin and Q.-L. Zhu, *Inorg. Chem.*, 2025, **64**, 17659–17665.
16 Y. Yu, S. Zhang, H. Wu, Z. Hu, J. Wang, Y. Wu and H. Yu, *J. Am. Ceram. Soc.*, 2024, **146**, 26081–26094.
17 K. Li, H. Wu, H. Yu, Z. Hu, J. Wang and Y. Wu, *Chem. Commun.*, 2024, **60**, 12734–12737.
18 A. L. Xu, M.-Y. Ran, X.-T. Wu, H. Lin and Q.-L. Zhu, *Coord. Chem. Rev.*, 2025, **540**, 216775.
19 L. Wang, H. Luo, S. Chen, L. Huang, L. Cao, X. Dong and G. Zou, *Cryst. Growth Des.*, 2025, **25**, 7803–7809.
20 R.-L. Tang, W. Yue, Y.-L. Lv, B.-W. Miao, W. Liu and S.-P. Guo, *Chem. Sci.*, 2025, **16**, 22021–22028.
21 Z. Bai and K. M. Ok, *Angew. Chem.*, 2024, **136**, e202315311.
22 H. Qiu, R. An, C. Cui, Z. Li, J. Yang, X. Wang, X. Hou, J. Li, J. Lu, J. Sun, Z. Yang, S. Pan and M. Mutailipu, *Angew. Chem., Int. Ed.*, 2025, **64**, e202507171.
23 Z. Chen, C. Li, X. Wu, J. Lu, Z. Yang, X. Hou and M. Mutailipu, *Aggregate*, 2025, **6**, e70134.
24 R. L. Tang, B. W. Miao, G. R. Zhu, W. Liu and S. P. Guo, *Adv. Sci.*, 2025, **12**, e15170.
25 R. L. Tang, W. Y. Gao, G. R. Zhu, Y. Chi, L. Ma, W. Liu and S. P. Guo, *Angew. Chem., Int. Ed.*, 2026, **65**, e21066.
26 Y. L. Lv, R. L. Tang, L. Ma, C. Chen, W. Liu and S. P. Guo, *Adv. Opt. Mater.*, 2025, **13**, e01839.
27 R.-L. Tang, D.-X. Yang, J.-D. Guo, C. Chen, W. Liu and S.-P. Guo, *Sci. China: Chem.*, 2026, **69**, 1–6.
28 P. Ramasami and J. S. Murray, *J. Mol. Model.*, 2024, **30**, 81.
29 Z. Chen and M. Mutailipu, *Chin. J. Struct. Chem.*, 2025, **44**, 100695.
30 P. G. Harrison, B. J. Haylett and T. J. King, *Inorg. Chim. Acta*, 1983, **75**, 259–264.
31 P. Geerlings, F. De Proft and W. Langenaeker, *Chem. Rev.*, 2003, **103**, 1793–1874.
32 J. P. Perdew, K. Burke and M. Ernzerhof, *Phys. Rev. Lett.*, 1996, **77**, 3865.
33 A. Yamaguchi, R. Penland, S. Mizushima, T. Lane, C. Curran and J. Quagliano, *J. Am. Chem. Soc.*, 1958, **80**, 527–529.
34 J. P. Singh, S. Pal, Y. K. Sharma and A. Nag, *J. Opt.*, 2024, **53**, 4845–4852.
35 B. K. Patel, S. Rath, S. N. Sarangi and S. N. Sahu, *Appl. Phys. A: Mater. Sci. Process.*, 2007, **86**, 447–450.
36 Q. Zhang, X. Liu, M. I. B. Utama, J. Zhang, M. de la Mata, J. Arbiol, Y. Lu, T. C. Sum and Q. Xiong, *Nano Lett.*, 2012, **12**, 6420–6427.
37 Z. Zhao, R. V. Goncalves, S. K. Barman, E. J. Willard, E. Byle, R. Perry, Z. Wu, M. N. Huda, A. J. Moulé and F. E. Osterloh, *Energy Environ. Sci.*, 2019, **12**, 1385–1395.
38 B. Boruah, R. Gupta, J. M. Modak and G. Madras, *J. Jordan Phys.*, 2019, **1**, 2748–2760.
39 L.-J. Ding, X.-T. Zhang, X.-Y. Guo, Y. Xue, C.-Q. Lin and D. Huang, *Acta Phys. Sin.*, 2023, **72**, 013101.
40 A. Sarma, A.-C. Dippel, O. Gutowski, M. Etter, M. Lippmann, O. Seeck, G. Manna, M. K. Sanyal, T. F. Keller and S. Kulkarni, *RSC Adv.*, 2019, **9**, 31900–31910.
41 J. Guo, A. Tudi, S. Han, Z. Yang and S. Pan, *Angew. Chem., Int. Ed.*, 2019, **58**, 17675–17678.
42 Y. Chen, H. Luo, Z. Yin, X. Dong, D. Gao, Y. Zhou, L. Huang, L. Cao and G. Zou, *Inorg. Chem.*, 2024, **63**, 15206–15214.
43 P.-F. Li, X.-L. Liu, S.-Q. Zhou, M.-C. Wang, J.-J. Wu, Y.-W. Zhong and J. Yao, *Dalton Trans.*, 2025, **54**, 17189–17195.
44 S. Liu, X. Ma, X. Long and Y. Yang, *Chin. J. Chem.*, 2025, **43**, 2623–2629.
45 Q. Li, H. Mi, L. Yang, H. Sha, D. Yang, Z. Wang, R. Su, B. Su and C. He, *J. Mater. Chem. C*, 2025, **13**, 10671–10675.
46 J. P. Perdew, K. Burke and M. Ernzerhof, *Phys. Rev. Lett.*, 1996, **77**, 3865–3868.